

Comparison of He I line intensity ratio method and electrostatic probe for electron density and temperature measurements in NAGDIS-II

Shin Kajita

Graduate School of Engineering, Nagoya University, Nagoya 464-8603, Japan

Noriyasu Ohno

EcoTopia Science Institute, Nagoya University, Nagoya 464-8603, Japan

Shuichi Takamura

Graduate School of Engineering, Nagoya University, Nagoya 464-8603, Japan

Tomohide Nakano

Japan Atomic Energy Agency, Ibaraki 311-0193, Japan

(Received 25 October 2005; accepted 14 December 2005; published online 25 January 2006)

The electron density and temperature obtained from the line intensity ratio method of He I ($\lambda=667.8, 706.5,$ and 728.1 nm) are compared to the probe method in a divertor simulator. When a collisional radiative model that does not include the effect of the radiation transport was used for the analysis, n_e obtained from the spectroscopic method was significantly higher than that from the electrostatic probe method. The discrepancy between the two methods increases with the gas pressure; in other words, it increases with the optical thickness. In the case that the effect of the radiation trapping is taken into consideration using optical escape factor, the discrepancy becomes moderate. And then, the parameters obtained from the line intensity ratio method agree with the probe method within a factor of 2 in the case that the radiation trapping was introduced with $R=0.05$ m, which corresponds to the column radius of the spatial profile of the excited population density. In recombining plasmas, however, it was shown that the line intensity ratios might not be appropriate because the recombining component broke the monotonic increase/decrease dependences of the line intensity ratios on n_e and T_e . A measurement of another He I line intensity of 447.1 nm ($2^3P \leftarrow 4^3D$) is proposed for solving the problem. © 2006 American Institute of Physics.

[DOI: [10.1063/1.2164461](https://doi.org/10.1063/1.2164461)]

I. INTRODUCTION

Electron temperature, T_e , and density, n_e , are important parameters for understanding the divertor physics of experimental fusion devices. Electrostatic probe method and laser Thomson scattering (LTS) method¹ have been used for the measurement of these parameters. However, former method could suffer damages due to high heat and particle fluxes, and latter method requires good accessibility to the divertor region. Further, in detached plasmas where the heat and particle fluxes are reduced accompanied with the plasma recombination, the current-voltage characteristics of the single probe become anomalous.² As for the LTS method, the separation of the Thomson scattering signal from the stray light may be hard since the width of the Doppler broadening becomes narrow owing to low electron temperature. Passive spectroscopies in combination with an appropriate model for the excited population distribution could be alternative methods. Since helium particles are produced by fusion reaction, and the density becomes 5%–10% of the total particle density in divertor region,³ helium line intensity ratios can be applicable and convenient for the measurement in the divertor region.

With regards to He I, a collisional radiative (CR) model has been provided,^{4,5} and some line intensity ratios have

been applied for the measurements. One candidate for the combinations of the line intensities is $\lambda=728.1$ nm ($2^1P \leftarrow 3^1S$), $\lambda=667.8$ nm ($2^1P \leftarrow 3^1D$), and $\lambda=706.5$ nm ($2^3P \leftarrow 3^3S$), which have been first proposed in Ref. 6. So far, n_e and T_e measurements based on the CR model using the line intensity ratios have been applied in TEXTOR (Tokamak Experiment for Technology Oriented Research, Jülich, Germany),⁶ JET (Joint European Torus, Abingdon, UK),^{7,8} JT-60U (Japan Atomic Energy Research Institute Tokamak-60 Upgrade, Naka, Japan),⁹ RFX (Reversed Field experiment, Padova, Italy),¹⁰ TJ-II stellarator (Madrid, Spain),^{11,12} and LHD (Large Helical Device, Toki, Japan).⁵ Although the spectroscopic method deduced consistent value with other measurement method in some literatures, it has been recently reported from the results in linear divertor simulators that the effects of radiation trapping on the population distribution of helium atoms are considerable.^{13,14} In Ref. 13, the effects of the radiation trapping are observed as the enhancement of the intensity ratio of 501.6 nm ($2^1S \leftarrow 3^1P$)/ 492.2 nm ($2^1P \leftarrow 4^1D$) in NAGDIS-I (Nagoya, Japan). In Ref. 14, the enhancement of the population densities in n^1P and n^1D states (n is the principal quantum number), which are relevant to the line intensity of 728.1 and 667.8 nm, are explained by the effect of the radiation trap-

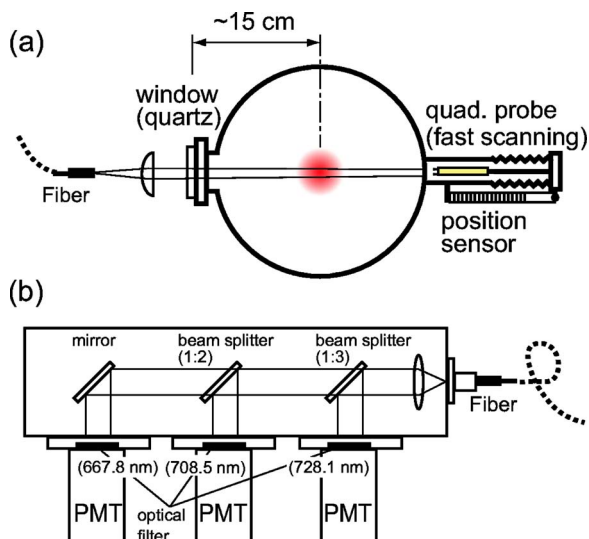


FIG. 1. (Color online) (a) Schematic of the experimental setup in the NAGDIS-II and (b) schematic view of the spectroscopy.

ping in MAP-II (Tokyo, Japan). Because the radiation trapping may pose problems for the evaluation of n_e and T_e , it is necessary to investigate the validity of the method and the limitation for the practical application with the inclusion of the effect of the radiation trapping.

In the present article, the electron density and temperature evaluated from the line intensities 728.1, 706.5, and 667.8 nm are compared with those from the electrostatic probe in a divertor simulator NAGDIS-II (NAGGoya Divertor Simulator). By investigating the dependences of n_e and T_e on the radial position, discharge current and gas pressure, the effects of the radiation trapping of the resonance lines ($1^1S \leftarrow n^1P$) on the evaluation of n_e and T_e are discussed. A filter spectrometer using interference filters and photomultiplier tubes (PMTs), which has a great time resolution ($\leq 10^{-6}$ μ s), was used in this study as shown in Sec. II A; thus, the effect of the temporal evolution of the emission is discussed additionally.

The experimental setup and analysis method are shown in Sec. II. The results and discussion about the temporal evolution of the emission and radial emission profile are given in Sec. III A and III B, respectively. The discharge current and gas pressure dependences of n_e and T_e are given in Sec. III C. In Sec. III D several problems for the practical application to recombining plasmas related to plasma detachment are presented. Finally, the paper is concluded in Sec. IV.

II. EXPERIMENTAL SETUP AND ANALYSIS METHOD

A. Experimental setup

The experiments were performed in the divertor simulator NAGDIS-II. The detail description of NAGDIS-II can be found, for example, in Refs. 15 and 16. Figure 1(a) shows the schematic view of the cross section of the NAGDIS-II. Helium plasmas were generated in the source region, and additional helium gas was injected into the downstream re-

gion. The distance between the plasma source and the measurement region was ~ 2 m. The strength of the magnetic field, which was formed by 21 solenoidal coils, was ~ 0.1 T at the measurement region. An object lens with a focal length of 50 mm collimates the line of sight of an optical fiber. The spatial resolution was ~ 5 mm. The spatial profile of the emission was measured by moving the optical system in the perpendicular direction to the plasma column using a movable stage.

The light from the plasma was transmitted to a spectroscopy, which is shown in Fig. 1(b), through the optical fiber, and then, split into three parts using two beam splitters and a mirror. In order to measure the He I line intensities, interference filters with the center wavelengths of the transmission bands of 667.8, 706.5, and 728 nm, and the full width at half-maximum (FWHM) of ~ 1.5 nm were equipped in front of the three PMTs. The optical chains beam splitters plus interference filters plus PMTs were relatively calibrated by comparing the intensities to those of another spectroscopy, which was calibrated with a standard light source.

Regarding the electrostatic probe measurement, a modified triple probe technique¹⁷ with four probe tips was used. Two of the four electrodes were used for floating double probe system, while the averaged potential of the two other floating electrodes were used for the floating potential measurement to compensate potential gradient. The floating electrode for the double probe was constantly biased 100 V to each other. The configuration of the four electrode was aligned so that the electrodes were not located on the same magnetic field line with each other. The position of the probe was measured with a position sensor.

One of the advantages of these measurement systems is time resolution that is high enough to be applicable to measure the fluctuations. Although, in the present study, the detail analysis of the fluctuations of n_e and T_e is beyond the scope, the time evolution of the emission intensities are taken into account when the average and error values of n_e and T_e are derived.

The effect of the high energy electrons is quite important under some conditions¹³ both on spectroscopic and probe methods. However, in NAGDIS-II, the effects of the high temperature electrons or energetic beam electron components are negligible at least under the condition in the present paper. This may be because the neutral pressure at the plasma source region in NAGDIS-II is considerably high (~ 1 Torr) and the electron density is sufficiently high to mitigate the energetic electrons. Figure 2 shows a typical probe characteristics in NAGDIS-II. The naturalized logarithm of the probe current is presented as a function of the probe voltage. The helium neutral pressure was ~ 3 mTorr, and the discharge current and the voltage was 30 A, and 65 V, respectively. The probe current was nicely fitted using single temperature with Maxwell distribution function as the solid line in Fig. 2. No evident indication of the high-energy electrons can be seen. Even if the high energy components existed, the ratio of the high energy components are much less than 1%. Therefore, in the present paper, the effects of the high-energy electron component are not important, so that they are neglected for the analysis.

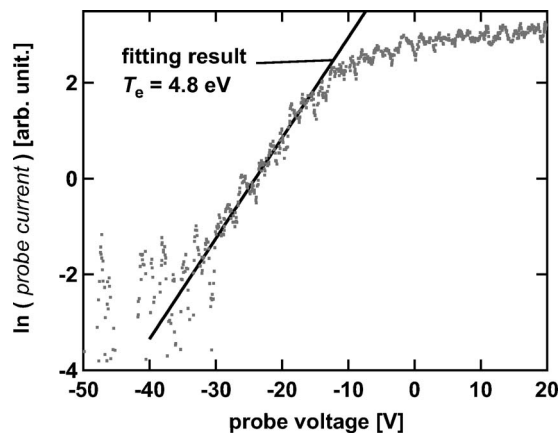


FIG. 2. Typical single probe characteristics in NAGDIS-II. Dots are the naturalized logarithm of the probe current, solid line is the fitting result with single electron temperature (4.8 eV).

B. Spectroscopic method

In order to determine n_e and T_e from the spectroscopic method, the measured intensity ratios, 667.8/728.1 and 728.1/706.5 nm, are compared to those obtained from the CR model.⁵ Then, n_e and T_e are evaluated such that the sum of the differences between the intensity ratios from the experiment and those from the calculation [i.e., the value f of Eq. (41) in Ref. 5] becomes minimum.

In this article, the formulation II in Ref. 5, in which two metastable states are also treated with quasi-steady-state approximation, was used. This approximation was reasonable in our experimental regime. Given that the radius of the plasma column is 0.05 m and the gas temperature is 300 K, the characteristic time for the transport of helium atom become $\sim 50 \mu\text{s}$. On the other hand, the lifetime of the metastable states, which can be evaluated using the CR rate coefficients as explained in Sec. III B, are shorter than $1 \mu\text{s}$ in the experimental regimes. Because the lifetime of the metastable states are much shorter than the characteristic time for the transport, the effect of the transport is negligible in our experimental regimes. Therefore, the formulation II is appropriate in this study, and the densities of the metastable states are determined by balancing the production rate, which is functions of ground state atomic density, and electron density and temperature, with the destruction rate, determined by electron collision processes.

Figure 3 shows the electron temperature dependence of the ion density ratio to neutral density, n_i/n_0 , at ionization equilibrium calculated using the CR model for $n_e=10^{11}$ and 10^{13} cm^{-3} . The neutral particle pressure was assumed to be 5 mTorr. The ionizing plasmas exist below (or right-hand side of) the line, whereas the region above (or left-hand side of) the line corresponds to recombining plasmas. Because the electron temperature was above 4 eV at the plasma center under the experimental conditions in this study, only the ionizing components were used for the analysis. The effect of the recombining components are separately discussed in Sec. III D.

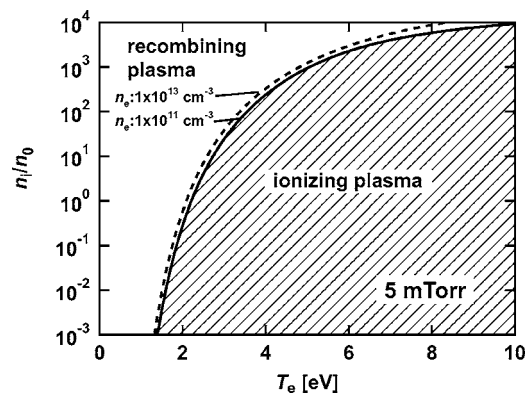


FIG. 3. Electron temperature dependence of the ion density ratio to the neutral density, n_i/n_0 , at ionization equilibrium calculated using the CR model for $n_e=10^{11}$ and 10^{13} cm^{-3} . Helium neutral pressure of 5 mTorr is assumed.

C. Radiation trapping

It has been pointed out that the optical depths for the resonance lines ($1^1S \leftarrow n^1P$) become thick in typical helium discharge plasmas.^{13,14} In these cases, the singlet P populations are enhanced due to the absorption of the resonance lines. The effect of the photon transport on the population of the excited states can be taken into consideration by introducing an optical escape factor g_0 , such that the spontaneous emission coefficient A decreases to g_0A . The value of g_0 is estimated by following formula¹⁸:

$$g_0 \sim \frac{1.92 - 1.3/[1 + (\kappa_0 R)^{6/5}]}{(\kappa_0 R + 0.62)[\pi \ln(1.357 + \kappa_0 R)]^{1/2}}, \quad (1)$$

where R is the radius of the spatial distribution of the excited atom, and κ_0 is the absorption coefficient at the center of the spectrum having a Gaussian profile, written as

$$\kappa_0 = \frac{e^2}{4Mc\epsilon_0\Delta\omega_D\sqrt{\pi}} n(p)f_{p,q}. \quad (2)$$

Here, M is the mass of the atom; c , velocity of light; ϵ_0 , dielectric constant in vacuum; $\Delta\omega_D$, width of the absorption line; $n(p)$, density of the lower state; and $f_{p,q}$, oscillator strength for the transition p (lower state) $\rightarrow q$ (upper state). In the derivation process of the escaping factor presented in Eq. (1), it is assumed that the spatial distribution of the excited helium atoms is parabolic one, in which the population density becomes zero at $r \sim R$. It is noted that the value is appropriate only at the center of the plasma column, thus it may not be appropriate when applied to the peripheral region. It is difficult to determine the optimum R at the moment, so that we used R of 0.05 m, which corresponds to the plasma radius where the electron density reduced to $\sim 1\%$ of the central density.

Figure 4 shows the gas pressure dependence of the absorption coefficients κ_0 for the helium resonance lines $1^1S \leftarrow 2^1P$, $1^1S \leftarrow 3^1P$, and $1^1S \leftarrow 4^1P$. Because the effect of the radiation trapping begins to appear from $\kappa_0 R \sim 0.1-1$,¹⁸ the effect is expected to be significant even if the gas pressure is lower than 1 mTorr in NAGDIS-II. This result also

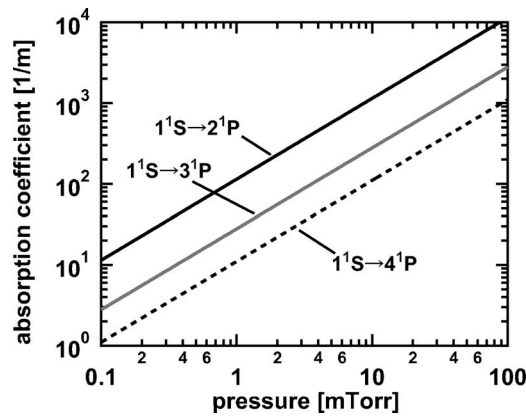


FIG. 4. Gas pressure dependences of the absorption coefficients at the center of the helium spectrum, $1^1S \leftarrow 2^1P$, $1^1S \leftarrow 3^1P$, and $1^1S \leftarrow 4^1P$. Gas temperature of 300 K is assumed.

indicates that, the effect of the radiation trapping is not negligible even in experimental fusion devices if the partial pressure of the helium atom is not sufficiently low.

D. Abel inversion

In order to obtain the local emission profile from the line-integrated emission, Abel inversion method was used. For the sake of reducing the numerical disturbance due to the experimental error, the line-integrated emission profile, $I(y)$, was first fitted to the function

$$I(y) = \left(\sum_{n=0}^N a_n y^{2n} \exp(-\alpha y^2) \right), \quad (3)$$

where y is the minimum distance between the line of sight and column center, and a_n and α are coefficients. In Eq. (3), $N=3$ is used in terms of minimizing the fitting error. Then, the local emission profile $\epsilon(r)$ was deduced as follows¹⁹:

$$\epsilon(r) = -\frac{1}{\pi} \int_r^R \frac{I'(y)}{(y^2 - r^2)^{1/2}} dy, \quad (4)$$

where R corresponds to the radius of the emission profile.

III. RESULTS AND DISCUSSION

A. Effect of temporal evolution

Figures 5(a) and 5(b) show the temporal evolutions of n_e and T_e , respectively, obtained from the spectroscopic method. The time resolution is generally limited by the response of the PMTs or electric circuit or sampling frequency of the analog-to-digital converter (ADC). In Fig. 5, the time resolution was limited by the ADC sampling frequency of 100 kHz, since it was much slower than the response of the PMTs and electric circuit (≥ 1 MHz). The emission was measured at $y=0$ (line-integrated emission through the plasma center). The effect of the radiation trapping was introduced using $R=0.05$ m for the analysis. We can observe the fluctuations of n_e and T_e in Figs. 5(a) and 5(b), respectively. Although the fluctuations are also observed using the triple probe method, the fluctuation levels, \tilde{n}_e/n_e or \tilde{T}_e/T_e ,

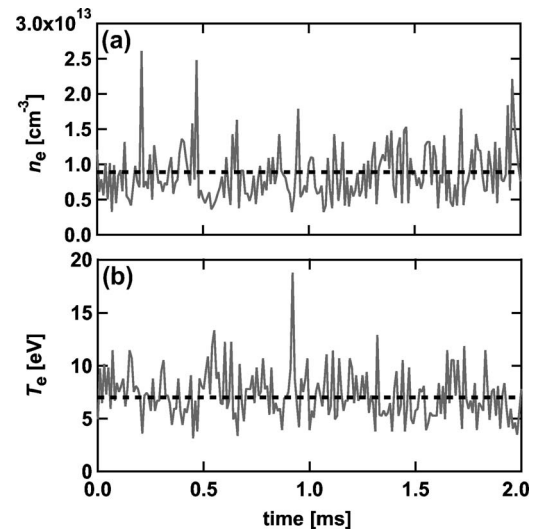


FIG. 5. Temporal evolution of (a) electron density and (b) temperature obtained from spectroscopic method. The effect of the radiation trapping was taken into account with $R=0.05$ m.

deduced from the spectroscopic method are somewhat larger than those from the probe method. We speculate that this may be attributed to the line-integral effect of the emission. Because the fluctuation level at the peripheral region is greater than that at the central region in NAGDIS-II,²⁰ line-integrated emission intensity may provide greater fluctuation level on the measurement.

Averaged values of n_e and T_e were obtained by two ways in the present study. In the first way, n_e and T_e are evaluated for ~ 5000 data points, and then, averaged value are deduced from them. In the second way, the line intensities are averaged at first, and then, n_e and T_e are obtained from the averaged line intensities. In the case of the results in Fig. 5, the averaged values of n_e and T_e obtained from the first method were $8.9 \times 10^{12} \text{ cm}^{-3}$ and 7.0 eV, respectively. In addition, the standard deviation of n_e and T_e , i.e., \tilde{n}_e and \tilde{T}_e , were estimated to be $4.1 \times 10^{12} \text{ cm}^{-3}$ and 2.1 eV, respectively. In the latter method, the deduced n_e and T_e were $7.9 \times 10^{12} \text{ cm}^{-3}$ and 6.9 eV, respectively. Although the differences between the two ways were negligible under this condition, significant deviation appears in some cases. In the present article, we call the former way as “temporal evolution analysis,” and the latter way as “emission averaging analysis.”

B. Radial profile

Figure 6 shows a typical emission profile of the line intensity of 706.5 nm. Open circles and dotted line show the measured line intensity and fitting result using Eq. (3), respectively. Solid line represents the local emission intensity reconstructed using the Abel inversion method. The emission profile has a peak at the center, and the emission intensity becomes half of the central intensity at ~ 8 mm. For other line intensities, i.e., the intensities of 667.8 and 728.1 nm, the spatial profile has similar dependences with that for 706.5 nm.

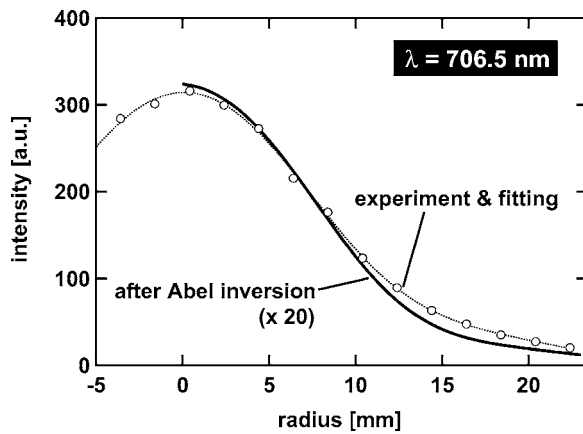


FIG. 6. The spatial profile of the line intensity of 706.5 nm. Open circles and dotted line show the measured line intensity and fitting result, respectively. Solid line shows the local emission intensity reconstructed using the Abel inversion method.

Dots in Figs. 7(a) and 7(b) show the radial profiles of electron density and temperature, respectively, obtained from the probe method. The discharge voltage and current were 68 V and 30 A, respectively, and the helium neutral pressure was 1.5 mTorr at the measurement region. The electron density and temperature at the plasma center were about $2 \times 10^{12} \text{ cm}^{-3}$ and 7 eV, respectively. Both of the density and temperature decreased as increasing the distance from the center of the plasma column, r , and the density was approximately half at $r \sim 15 \text{ mm}$.

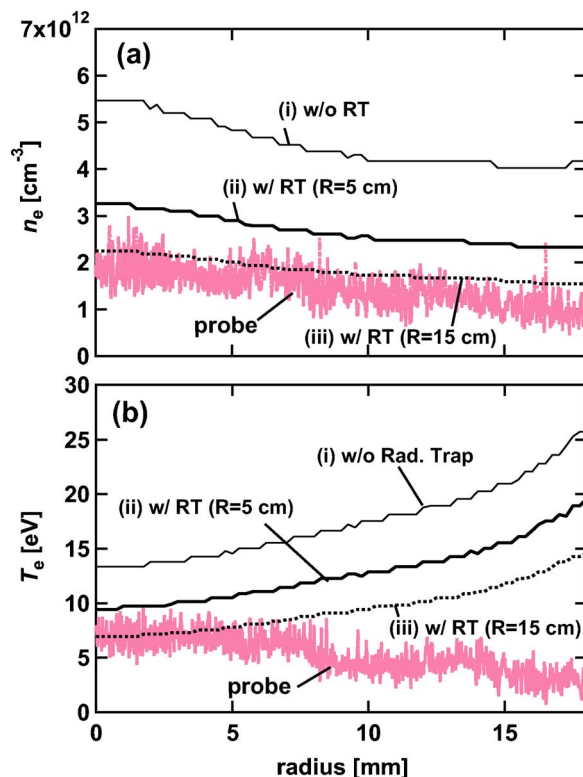


FIG. 7. (Color online) Radial profiles of (a) electron density and (b) temperature. Dots are the results obtained from electrostatic probe, and solid and dotted lines (i)–(iii) are the results obtained from spectroscopic method.

Solid lines of case (i) in Figs. 7(a) and 7(b) show the spatial profile of n_e and T_e obtained from the local emission intensity reconstructed using the Abel inversion method. Both of the density and temperature obtained from the spectroscopic method were higher than those from the probe method. Moreover, the temperature increased with r unnaturally. Solid lines of cases (ii) and (iii) in Fig. 7 are the results including the effect of the radiation trapping for the resonance lines with $R=0.05$ and 0.15 m (radius of vacuum chamber), respectively, assuming the gas temperature of 300 K. The differences between the probe and spectroscopic method become moderate when the radiation trapping is taken into account. The results of case (iii) well agree to the probe method at the central position. However, there is an assumption with regard to the spatial profile of $n(p)$ in the derivation process of Eq. (1), so that it is difficult to conclude that the size of the vacuum chamber (0.15 m) is appropriate for R at the moment. Although it is difficult to discuss the sensitivity quantitatively at present, one can say that the model is useful for mitigating the influence of the radiation trapping on n_e and T_e measurements. If the spatial distributions of the excited atomic density were determined by measuring the emission from the excited atoms, or by using theoretical or numerical modeling, the detailed investigation of the escaping factor is possible. These quantitative investigations including the spatial profiles of $n(p)$ are remained as our future work.

On the other hand, regarding the increasing tendency of the temperature with r on the spectroscopic method, the tendency was not compensated even if the radiation trapping was introduced. The transport effect of metastable states of helium atom (2^1S and 2^3S) was one of the candidates to cause this discrepancy. However, they could not explain the observed tendency, as investigated later. Using the formulation II where the transport effect was neglected, the densities of 2^1S state and 2^3S state at $r=0 \text{ mm}$ are evaluated to be $n_{2^1S}(0 \text{ mm})=1.8 \times 10^9 \text{ cm}^{-3}$, and $n_{2^3S}(0 \text{ mm})=5.7 \times 10^{10} \text{ cm}^{-3}$, respectively, whereas those at $r=25 \text{ mm}$ are evaluated to be $n_{2^1S}(25 \text{ mm})=5.1 \times 10^6 \text{ cm}^{-3}$, and $n_{2^3S}(25 \text{ mm})=2.0 \times 10^8 \text{ cm}^{-3}$, respectively. These results show that the densities of the metastable states of helium atom at the peripheral region was several hundreds times lower than those at the central region if the transport effect was not taken into account. The destruction rate of the metastable states can be evaluated as $n_e k_2 \text{ s}^{-1}$ for 2^1S state and $n_e k_3 \text{ s}^{-1}$ for 2^3S state, where k_2 and k_3 are the CR coupling coefficients defined in Ref. 5. Thus, if the metastable state densities at peripheral region are determined by the transport from the central region to the peripheral region, the densities can be roughly estimated as

$$n_{2^1S}(r) \sim n_{2^1S}(0) \exp(-n_e k_2 \tau), \quad (5)$$

$$n_{2^3S}(r) \sim n_{2^3S}(0) \exp(-n_e k_3 \tau), \quad (6)$$

where τ is the characteristic time of the transport. Assuming the gas temperature of 300 K, τ is obtained as $\sim 22 \mu\text{s}$ for the characteristic length of 25 mm. Using the plasma parameters at $r=0 \text{ mm}$, $n_e k_1$ and $n_e k_3$ are evaluated to be 5.1

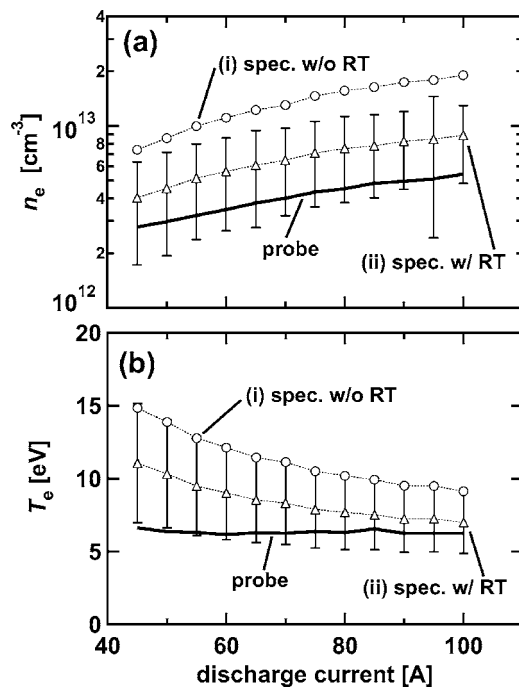


FIG. 8. Discharge current dependences of (a) electron density and (b) temperature. Solid lines and dotted lines (i)–(ii) are the results obtained from the probe and spectroscopic method, respectively.

$\times 10^6$ and $1.8 \times 10^6 \text{ s}^{-1}$, respectively. Based on these evaluations, we can easily estimate that values of Eqs. (5) and (6) are sufficiently smaller than measured n_{2^1S} (25 mm) and n_{2^3S} (25 mm), respectively. Thus, the increasing tendency of the temperature with r on the spectroscopic method cannot be explained by the transport of the metastable states of helium atom.

Although the reason to cause this tendency was not clear at the moment, we speculate that one of the reasons is also the effect of the radiation transport. Because the optical escape factor in Eq. (1) is local value at the center of the cylinder, Eq. (1) may not be appropriate at the peripheral region of the plasma column. Radiation from the central region may enhance the population of the singlet system at the peripheral region, and result in the overestimation of the temperature owing to the enhancement of the line intensity ratio of the singlet to the triplet. In future studies, it is necessary to introduce the geometrical effect by using direct simulation of photon transport based on Monte-Carlo method as shown in Ref. 21.

Comparing the results from line-integrated emission to the results from the local emission, the line-integrated emission reflects the values around the central region ($r \sim 0\text{--}5 \text{ mm}$). This is caused by the fact that the emission from the central region is greater than that from the peripheral region as shown in Fig. 6. Therefore, the results deduced from the line-integrated emission provide the parameters at central region unless the emission profile does not change significantly.

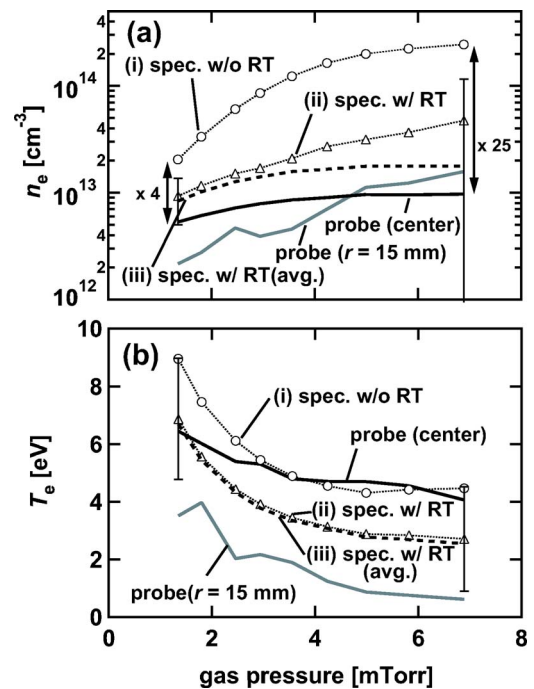


FIG. 9. Gas pressure dependences of (a) the electron density and (b) temperature. Solid lines are the results obtained from the probe method. The cases (i) open triangles, (ii) circles and (iii) dotted lines are the results obtained from the spectroscopic method. The cases (i) and (ii) present the results obtained with temporal evolution analysis, and the case (iii) presents the results obtained with emission averaging analysis.

C. Discharge current and gas pressure dependences

In this section, the dependences of n_e and T_e on the discharge current and gas pressure are discussed using the line-integrated emission. Figure 8 shows the discharge current dependences of (a) the electron density, and (b) temperature obtained from the probe (solid lines) and spectroscopic methods (open circles and triangles). In Fig. 8, n_e and T_e are evaluated with temporal evolution analysis. Cases (i) and (ii) correspond to the results without radiation trapping, and with radiation trapping using $R=0.05 \text{ m}$, respectively. Although the electron density in case (i) was about two to five times higher than that from the probe method, the discrepancy became moderate in the case that the effect of the radiation trapping was taken into consideration as shown in case (ii). Similarly, the electron temperature in case (i) was considerably higher than the probe method; the overestimation became moderate in case (ii).

Figure 9 shows the gas pressure dependences of (a) the electron density, and (b) temperature obtained from the probe (solid lines) and spectroscopic methods (open circles and triangles). Cases (i) and (ii) correspond to the results without radiation trapping, and with radiation trapping using $R=0.05 \text{ m}$, respectively, with temporal evolution analysis. The discrepancy between the probe method and spectroscopic one increases with the gas pressure in case (i). The electron density of case (i) was 4 times greater than that from probe method at $\sim 1.5 \text{ mTorr}$; at $\sim 7 \text{ mTorr}$, the value of case (i) became 25 times greater than that from the probe method. The increase of the discrepancy between the case (i) and the probe method can be attributed to the increase of the

effect of the radiation trapping, since κ_0 in Eq. (2) is proportional to the neutral density $n(p)$. Therefore, in the case that the radiation trapping was introduced [case (ii)], the discrepancy of n_e and the increase tendency of the discrepancy became moderate.

As for the electron temperature shown in Fig. 9(b), the spectroscopic method gives lower value than the probe method (center), in the case that the radiation trapping is taken into consideration. This might be attributed to the modification of the plasma spatial profile. As can be seen in Fig. 9(a), the electron density at the peripheral region increases with the gas pressure. We believe that the modification of the spatial profile of the electron density may cause the enhancement of the photon emission from the peripheral region where T_e is lower than the plasma center. We should note that, under high-pressure condition, T_e at the peripheral region is sufficiently lower than 2 eV, so that the plasma at the peripheral region may be in the recombining regime. On the other hand, the central region is remained to be ionizing phase. Therefore, the line-integrated emission contains mainly two emission components, namely, the emission from the central ionizing plasma and from peripheral recombining plasma. Since the separation of the two emission components from the line-integrated emission is impossible, it is difficult to discuss the effect of the recombining component at the moment. Further, the method itself has some problems when recombining components are included. The effects of the recombining components are separately discussed in Sec. III D. Although it seems to be true that the width of the density profile becomes greater as increasing the gas pressure, it is under investigation whether the peripheral density can be higher than the central density as shown in Fig. 9(a). It is necessary to examine the reproducibility of the experimental results, and the validity of the triple probe method in plasmas with bursty fluctuations.²⁰

The error bars were represented at ~ 1.5 and 7 mTorr in cases (ii) of Figs. 9(a) and 9(b). The fluctuation components \tilde{n}_e/n_e increased with the gas pressure, and \tilde{n}_e/n_e exceeded 100% in high pressure region (≥ 3 mTorr). We speculate that the increase of \tilde{n}_e/n_e is caused by the increase of the emission from the peripheral region where fluctuation level is greater than the central region in NAGDIS-II.²⁰ In Figs. 9(a) and 9(b), case (iii) (dotted line) shows n_e and T_e obtained with emission averaging analysis. When the pressure was over 3 mTorr where \tilde{n}_e/n_e is sufficiently large, the deviation between cases (ii) (temporal evolution analysis) and (iii) (emission averaging analysis) appeared. Although \tilde{T}_e/T_e increased with the gas pressure similarly, the increasing rate was moderate and the discrepancy between the case (ii) and (iii) did not appear under the experimental condition. When using a normal spectroscope that does not have the capability to trace the temporal evolution of the three line intensities simultaneously, the obtained value should correspond to case (iii). Although quantitative analysis of the fluctuation effect is difficult as far as the line-integrated emission is used, it can be said that one should take care when analyzing temporal evolution of the emission under the condition where

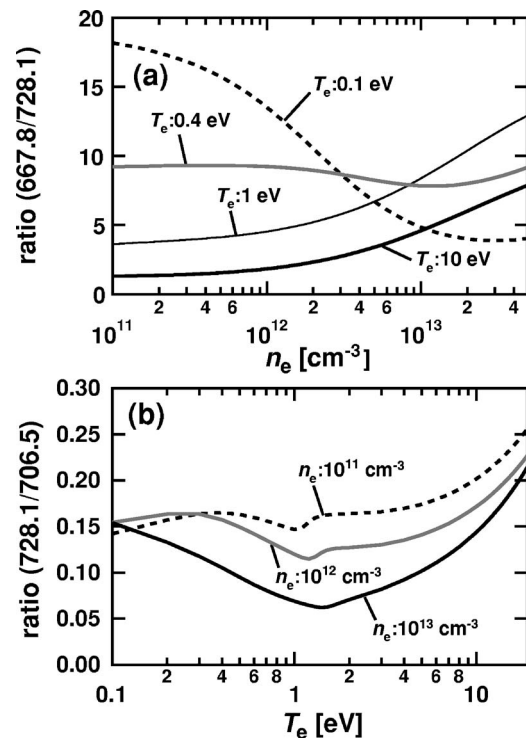


FIG. 10. Calculated line intensity ratios. (a) n_e dependence of the ratio 728.1/706.5 nm and (b) T_e dependence of the ratio 667.8/728.1 nm. The effect of the radiation trapping is not taken into account. The recombining components are included in the calculation.

the fluctuation level is high. The comparative studies of the fluctuation of T_e and n_e using the spectroscopic method and the probe method are our future work.

D. Practical application to recombining plasmas

Figure 10(a) is n_e dependence of the line intensity ratio of 667.8/728.1 nm at $T_e=0.1, 0.4, 1,$ and 10 eV. In these calculations, recombining components are included and the effect of the radiation trapping is not taken into account. Additionally, the gas pressure of 5 mTorr is assumed. At $T_e=1$ and 10 eV, the ratio monotonically increases with n_e , indicating that the ratio is appropriate for the evaluation of n_e . However, at $T_e=0.4$ eV, the ratio is almost constant; moreover, at $T_e=0.1$ eV, the ratio monotonically decreases as increasing the density. This indicates that the ratio 667.8/728.1 nm changes significantly not only with n_e but also with T_e in low-temperature recombining plasmas; further, it is difficult to determine n_e from the ratio 667.8/728.1 nm if $T_e \sim 0.4$ eV. Figure 10(b) is the T_e dependence of the ratio 728.1/706.5 nm for $n_e=10^{11}, 10^{12},$ and 10^{13} cm⁻³. Although the ratio 728.1/706.5 nm monotonically increases with T_e when $T_e > 2$ eV, it decreases with T_e in the range 0.3-1 eV. This indicates that the number of the combinations of n_e and T_e for minimizing the sum of the differences between the calculation and the experiment can be more than two in some cases.

Therefore, when the recombining components are included for the analysis in low temperature plasmas ($T_e < 5$ eV), one should take care not to choose wrong combination of n_e and T_e even if the plasma was not in recombining

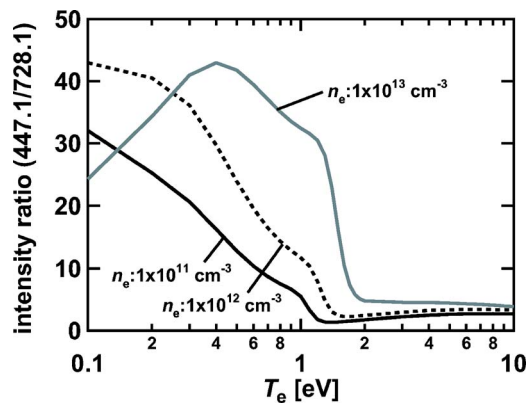


FIG. 11. Electron temperature dependences of the line intensity ratio 447.1/728.1 nm for $n_e = 1.0 \times 10^{11}$, 1.0×10^{12} and $1.0 \times 10^{13} \text{ cm}^{-3}$.

ing regime. For that purpose, it is important to distinguish whether the plasma is in the ionizing or recombining regimes. This problem may be solved by measuring another line intensity. Figure 11 shows the line intensity ratio of 447.1($2^3P \leftarrow 4^3D$)/728.1 nm as a function of T_e . In the calculation, helium gas pressure was assumed to be 5 mTorr, and the radiation trapping was not taken into consideration. We can see that the ratio is significantly enhanced in recombining phase ($T_e \lesssim 2 \text{ eV}$). Although, in high density plasmas ($\geq 10^{13} \text{ cm}^{-3}$), the intensity ratio decreases as decreasing the temperature when $T_e < 0.4$, the line intensity is very sensitive to the variation of T_e . Therefore, the line intensity ratio of 447.1/728.1 nm could be the indicator whether the plasma is in recombining or ionizing regime. This may help to solve the problem in recombining plasmas when determining the electron temperature using the line intensity ratios of 667.8/728.1 and 728.1/706.5 nm.

IV. CONCLUSION

The electron density and temperature obtained from the line intensity ratio method of He I ($\lambda = 667.8, 706.5, \text{ and } 728.1 \text{ nm}$) are compared to the probe method in divertor simulator NAGDIS-II. The analysis using the CR model that does not include the effect of the radiation transport deduced higher n_e than that from electrostatic probe method. The discrepancy between the two method increases with the gas pressure. The electron density from the spectroscopic method was 4 times greater than that from probe method at $\sim 1.5 \text{ mTorr}$; at $\sim 7 \text{ mTorr}$, the spectroscopic method deduced 25 times greater electron density than the probe method. This result indicates that the optical thickness increases with the gas pressure. In the case that the effect of the radiation trapping is taken into consideration using optical escape factor, the discrepancy becomes moderate. The electron density obtained from line intensity ratio method agree with the probe method within a factor of 2 in the case that the averaged emission intensities were used, and the radiation trapping was introduced with $R = 0.05 \text{ m}$, which corresponds to the column radius of the spatial profile of the excited population density.

For T_e measurement, although T_e was slightly overestimated, the effect of the radiation trapping was not so signifi-

cant in the case that the line integrated emission intensities were used. However, the spectroscopic method presented the increase dependence of T_e on radial position r . That was opposite dependence from that of electrostatic probe method. One of the reasons to cause this discrepancy is considered to be the radiation trapping. The radiation from the central region may enhance the population of the singlet system at the peripheral region, and results in the overestimation of the temperature at the peripheral region.

In recombining plasmas, the line intensity ratios might not be appropriate because the recombining component broke the monotonic increase/decrease dependence of the line intensity ratios on the n_e and T_e . The ratio 667.8/728.1 nm changes significantly not only with n_e but also with T_e . Further, in some cases, the number of the combinations of n_e and T_e for minimizing the sum of the differences between the calculation and the experiment can be more than two. We propose that measuring another He I line intensity of 447.1 nm ($2^3P \leftarrow 4^3D$) for solving the problem, because the line intensity ratio of 447.1/728.1 nm is very sensitive to T_e in low temperature region ($< 2 \text{ eV}$).

ACKNOWLEDGMENTS

Authors thank Dr. Goto from National Institute of Fusion Science (NIFS) for proving the CR model code. Authors also thank Dr. S. Kado and Mr. Y. Iida from the University of Tokyo, Dr. K. Sawada from the Shinshu University, and Dr. K. Nakamura from NIFS for useful advice and discussion. This work was supported in part by a Grant-in-Aid for Scientific Research from the Japan Society for the Promotion of Science (JSPS) Research Fellowships for Young Scientists (No. 17-7503).

- ¹T. N. Carlstrom, C. L. Hsieh, R. Stockdale, D. G. Nilson, and D. N. Hill, *Rev. Sci. Instrum.* **68**, 1195 (1997); A. Okamoto, S. Kado, S. Kajita, and S. Tanaka, *Rev. Sci. Instrum.* **76**, 116106 (2005).
- ²N. Ohno, N. Tanaka, N. Ezumi, D. Nishijima, and S. Takamura, *Contrib. Plasma Phys.* **41**, 473 (2001).
- ³G. Federici, C. Skinner, J. Brooks, J. Coad, C. Grisolia, A. Haasz, A. Hassanein, V. Philipps, C. Pitcher, J. Roth, W. Wampler, and D. Whyte, *Nucl. Fusion* **41**, 1967 (2001).
- ⁴T. Fujimoto, *J. Quant. Spectrosc. Radiat. Transf.* **21**, 439 (1979).
- ⁵M. Goto, *J. Quant. Spectrosc. Radiat. Transf.* **76**, 331 (2003).
- ⁶B. Schweer, G. Mank, A. Pospieszczyk, B. Brosda, and B. Pohlmeier, *J. Nucl. Mater.* **196–198**, 174 (1992).
- ⁷S. J. Davies, P. D. Morgan, Y. Ul'Haq, C. F. Maggi, S. K. Erents, W. Fundamenski, L. D. Horton, A. Loarte, G. F. Matthews, R. D. Monk, and P. C. Stangeby, *J. Nucl. Mater.* **241–243**, 426 (1997).
- ⁸Y. Andrew, S. J. Davies, D. Elder, L. D. Horton, G. F. Matthews, A. Meigs, P. D. Morgan, M. O'Mullane, M. Stamp, R. Prentice, and P. C. Stangeby, *J. Nucl. Mater.* **266–269**, 1234 (1999).
- ⁹H. Kubo, M. Goto, H. Takenaga, A. Kumagai, T. S. S. Sakurai, N. Asakura, S. Higashijima, and A. Sakasai, *J. Plasma Fusion Res.* **75**, 945 (1999).
- ¹⁰L. Carraro, G. D. Pol, M. E. Puiatti, F. Sattin, P. Scarin, and M. Valisa, *Plasma Phys. Controlled Fusion* **42**, 1 (2000).
- ¹¹B. Branas, D. Tafalla, F. L. Tabares, and P. Ortiz, *Rev. Sci. Instrum.* **72**, 602 (2001).
- ¹²E. de la Cal, *Plasma Phys. Controlled Fusion* **43**, 813 (2001).
- ¹³S. Sasaki, S. Takamura, S. Watanabe, S. Masuzaki, T. Kato, and K. Kadota, *Rev. Sci. Instrum.* **67**, 3521 (1996).
- ¹⁴Y. Iida, S. Kado, A. Okamoto, S. Kajita, T. Shikama, D. Yamasaki, and S. Tanaka, *J. Fusion Res.* (to be published).

- ¹⁵N. Ohno, D. Nishijima, S. Takamura, Y. Uesugi, M. Motoyama, N. Hattori, H. Arakawa, N. Ezumia, S. Krashennikov, A. Pigarov, and U. Wenzel, *Nucl. Fusion* **41**, 1055 (2001).
- ¹⁶S. Takamura, N. Ohno, D. Nishijima, and Y. Uesugi, *Plasma Sources Sci. Technol.* **11**, A42 (2002).
- ¹⁷S.-L. Chen and T. Sekiguchi, *J. Appl. Phys.* **36**, 2363 (1965).
- ¹⁸T. Fujimoto, *Plasma Spectroscopy* (Clarendon, Oxford, 2004).
- ¹⁹H. R. Griem, *Plasma Spectroscopy* (McGraw-Hill, New York, 1964).
- ²⁰N. Ohno, V. Budaev, K. Furuta, H. Miyoshi, and S. Takamura, *Contrib. Plasma Phys.* **44**, 222 (2004).
- ²¹Y. B. Golubovskii, I. A. Porokhova, H. Lange, S. Gortchakov, and D. Uhrlandt, *Plasma Sources Sci. Technol.* **14**, 45 (2005).